Amorphous-Crystal phase transition in Silicon nanoparticles embedded in amorphous SiO_2 matrices

Sergio Orlandini

Department of Chemistry,

University of Rome "Sapienza" Piazzale Aldo Moro 5,

00185 Roma, Italy

and

Consorzio Interuniversitario per le Applicazioni di

Supercalcolo Per Universitá e Ricerca (CASPUR),

Via dei Tizii 6, 00185 Roma, Italy

Host:
Giovanni Ciccotti
School of Physics,
Engineering and Material Science Building,
University College Dublin (UCD), Belfield, Dublin, Ireland

I. FINAL SCIENTIFIC REPORT

The purpose of my visit in University College of Dublin was to develop a methodology for the study of the phase diagram of confined nano-sized systems. The system in consideration consists of nanoparticles of Silicon embedded in a matrix of amorphous Silicon dioxide. We decide to study this system because it is emerging as one of the material of election for optoelectronics and for photovoltaic applications.

In this project I have studied the transformation of the Silicon nanoparticles embedded in amorphous SiO_2 from the amorphous phase to the crystal one by means of atomistic simulations. The time scale of this process largely exceed the timescale reachable by molecular simulations. However, recent progress on rare events provided techniques for overcoming the timescale problem. In our project we use the Temperature Accelerated Molecular Dynamics [12] and thermodinamic integration in order to obtain the free energy profile.

Despite the use of an accelerated molecular dynamic our results converge very slowly. During this period at UCD I have solved this problem combining the accelerated molecular dynamic with the replica exchange method [13].

The replica exchange method consists in running several simulations at different temperatures and to simultaniously swap the configurations between two parallel runs. The swapping is accepted according to a Metropolis criterion. The procedure consists of running different indipendent biased molecular dynamic simulations at different temperatures. After a fixed time we try to swap the configuration at different temperature. I have fixed a procedure to highly parallelize this method. Indeed, there are two level of parallelization in this method. One to the level of the molecular dynamics simulations and the other to control the swapping of the indipendent molecular simulations. Each molecular dynamic simulation is a parallel run implemented by the Message Passing Interface. Each simulation was ran on

eight cores. The swapping between the molecular dynamic simulations was implemented at a level of scripting language. The complete replica exchange and biased molecular dynamic simulation was executed on 64 cores.

II. INTRODUCTION

Nano-scale systems behave differently than ordinary bulk materials since, among other reasons, their physico-chemical properties do depend upon their size and shape. Considerable effort is ongoing to understand, design, fabricate, and manipulate materials at such a small length scale, so as to get tailored properties. In particular, the identification of how the structural features depend upon the actual thermodynamic conditions is attracting an increasing interest as it paves the way toward explaining the structure-property relationship, an issue of large technological impact. Among the nano-sized systems of technological interest, semiconductor nano-particles embedded in amorphous matrices are especially important for their possible application as photo-emitting materials for optoelectronics as well as materials for the light harvesting component of solar cells.

A feature strongly affecting the properties of nano-sized semicondutor particles is whether they are crystalline or amorphous. In particular, it has been experimentally observed that the photoluminescence intensity of Si nano-particles embedded in silica strongly depends (both in wavelength and intensity) on their crystallinity. Their structural evolution has been accordingly characterized: Si nano-particles are initially formed amorphous and then transformed into crystalline upon thermal annealing at high temperatures (typically at 1100°C or above) [2–6]. During annealing, another phenomenon has been nevertheless observed (namely the growth of nano-particles) which makes it difficult to unambiguously identify the actual atomistic mechanisms driving the observed evolution. Two models have been proposed to explain the experimental results: i) the system is always at the thermodynamic equilibrium state, but such a state could correspond to either a disordered or to an ordered atomic architecture, depending on the size of the nano-particles; ii) alternatively, the system is initially formed in the metastable disordered state, then evolving into the more stable crystalline one. In this latter case it is also assumed that the ordered phase is the most stable one for any nano-particle size (a typical bulk-like behavior), although the nano-particle is assumed to initially form in the amorphous state since this configuration is kinetically

favored. Evolution towards the crystalline state is eventually observed provided that the temperature is high enough to overtake the free energy barrier separating the disordered from the ordered phase.

In this paper we elaborate a fully atomistic theoretical explanation of the observed microstructure evolution of an embedded Si nano-particle, by performing computer experiments aimed at measuring its free energy in different states of aggregation. The main output of the present investigation is that we identify the most stable phase as a function of the particle size and the thermal conditions. This result is unprecedented and valuable on its own since it was unclear whether at the nanoscale the relative stability of the ordered and disordered phase is the same as in bulk samples. We show that this result is able to explain the experimental findings on the mechanism of formation of crystalline nano-particles [7]. In addition, we also fully characterize the atomic architecture of the nano-particle by calculating its pair correlation function g(r) and by analyzing the Steinhardt et al. $\mathcal{Q}_6$ bond-orientational order parameter [8] (see also Appendix). We shall demonstrate that standard theories of nucleation, such as the classical nucleation theory, are not able to model the formation mechanism of Si nano-particles in silica as the basic assumptions of these theories are violated.

III. THEORY

A. Sample preparation.

The computational samples are prepared by thermally annealing a periodically-repeated amorphous silica system, embedding Si nano-grains (extracted from a well equilibrates either amorphous or crystalline bulk). The amorphous silica sample was prepared through the quenching-from-the-melt procedure, that is by cooling down very slowly an high temperature SiO_2 melt. The atomic interactions are described by the environment-dependent classical force field by Billeter et al. [9, 10]. The reliability of this procedure and of the potential in modeling equilibrium and dynamical properties of Si nano-particles embedded in silica has been already established[11]. The total system contain from ≈ 6000 to ≈ 12000 particles, corresponding to a nano-particle radius varying in the range $1 - 2$ nm. Computational samples are first thermalized at 300 K in order to release possible stress at the Si/silica interface. Typically, during such a thermalization step, the nano-particles slightly shrink.

After this initial step, we impose the restraint on the size of the nano-particles (see below) and thermalize the samples at the various target temperatures. Because of the restraint on their size, at this stage we do not observe neither a further shrinking nor a growing of the nano-particles. After this treatment the samples are ready for the biased simulations described below. In order to verify possible artifacts due to finite-size effects, we repeated the calculations of the mean force at few selected value of $\mathcal{Q}_6^*$ (see below) on samples of different size of the silica matrix. We did not observe any significant difference in the mean force (the differences were within the statistical error). This demonstrates that there are no finite-size effects on our free energy calculations.

B. Free energy calculations.

We compute the free energy of a Si nano-particle as a function of its degree of order as measured by the bond-orientational order parameter ($\mathcal{Q}_6$) of Steinhardt et al. [8] (see also Appendix) calculated on the silicon atoms belonging to the nano-particle. For a disordered Si nano-particle $\mathcal{Q}_6$ is small (still not exactly zero due to finite size effects). On the contrary, in a crystalline object $\mathcal{Q}_6$ is much larger, and its actual value depends on the size. In practice, we perform the thermodynamic integration of the derivative of the free energy with respect the $\mathcal{Q}_6$ (hereafter referred to as "mean force"). The mean force is computed following the restraint method introduced by Maragliano and Vanden Eijnden [12] according to the expression

$$\frac{dF_T^k(\mathcal{Q}_6^*)}{d\mathcal{Q}_6^*} = \frac{1}{\tau}\int_0^\tau k\left[\mathcal{Q}_6(x(t)) - \mathcal{Q}_6^*\right] dt \tag{1}$$

where $dF_T^k(\mathcal{Q}_6^*)/d\mathcal{Q}_6^*$ is an approximation to the mean force at the value $\mathcal{Q}_6^*$, $x(t)$ is the all-atom configuration at the time t along a biased molecular dynamics (MD) trajectory generated at temperature T, and τ is the duration of the MD simulation. The parameter k in Eq. 1 determines the degree of biasing of the simulation (for $k = 0$ the MD simulation is unbiased). In the limit of $k \to \infty$, we get $dF_T^k(\mathcal{Q}_6^*)/d\mathcal{Q}_6^* \to dF_T(\mathcal{Q}_6^*)/d\mathcal{Q}_6^*$, where $F_T(\mathcal{Q}_6^*)$ is the free energy of the system in the state $\mathcal{Q}_6(x) = \mathcal{Q}_6^*$. In the present investigation, the biased MD is governed by the superposition of the physical potential (namely the Billeter et al. [9, 10] environment-dependent force field) and the biasing potential $k/2(\mathcal{Q}_6(x) - \mathcal{Q}_6^*)^2$ (please note that the k in this expression is the same as in Eq. 1) .

The above computational device holds valid for a bulk system. However, we are interested to investigate possible order-disorder transitions at a given (i.e. fixed) nano-particle dimension. Therefore, we have modified the above procedure by introducing the notion of size through the collective coordinate $\mathcal{R}(x)$, defined as the distance between the center x_c of the nano-particle (a point kept fixed during the simulations) and the closest oxygen atom, i.e. $\mathcal{R}(x) = \min |x_c - x_i^O|$, where x_i^O is the coordinate of the i-th oxygen atom. The biased MD described above is therefore modified by introducing a second biasing potential $k/2(\mathcal{R}(x) - \mathcal{R}^*)^2$. The integral given in Eq. 1 is therefore calculated along a biased MD in which $\mathcal{Q}_6$ and $\mathcal{R}$ are both restrained. We take advantage of this second collective coordinate to identify the Si atoms belonging to the nano-particle used in the calculation of the $\mathcal{Q}_6(x)$ collective coordinate. These atoms satisfy the condition $|x_c - x_i^{Si}| < \mathcal{R}^* - l$, where l is a parameter introduced to exclude the atoms at the frontier with the silica matrix ($l = 2.3$ Å in the present calculations). The second biasing potential gives rise to additional contributions to the interatomic forces which, unfortunately, cannot be straightforwardly evaluated since $\mathcal{R}(x)$ is a non-analytical function of x (and, therefore, there is no way to proceed through the direct calculation of $\nabla\mathcal{R}(x)$[12]). However, we were able to approximate $\mathcal{R}(x)$ by a smooth analytical function (see Appendix) and to perform biased MD runs according to this representation of $\mathcal{R}(x)$. By MD simulations biased both on $\mathcal{Q}_6$ and $\mathcal{R}(x)$, we have computed $dF_T(\mathcal{Q}_6^*; \mathcal{R}^*)/d\mathcal{Q}_6^*$ at several values of $\mathcal{R}^*$, keeping $\mathcal{R}^*$ fixed. By numerically integrating the $dF_T(\mathcal{Q}_6^*; \mathcal{R}^*)/d\mathcal{Q}_6^*$ over $\mathcal{Q}_6^*$ we eventually obtain $F_T(\mathcal{Q}_6; \mathcal{R}^*)$.

C. Improving the sampling of the configurational space.

Despite the use of biased MD, the calculation of $dF_T(\mathcal{Q}_6^*; \mathcal{R}^*)/d\mathcal{Q}_6^*$ through Eq. 1 resulted to converge very slowly for some values of $\mathcal{Q}_6^*$. This is because there can exist more than one metastable state in the domain of unbiased degrees of freedom corresponding to the same $\mathcal{Q}_6^*$ value. If these metastable states are separated by a free energy barrier larger than the thermal energy, then the ergodic hypothesis on the unbiased degrees of freedom at the basis of Eq. 1 is violated: therefore mean force cannot be accurately estimated via the biased MD described above. An example is offered by the two quasi-crystalline configurations shown in Fig. 1, corresponding to the same value of the $\mathcal{Q}_6$ parameter, but embedding different defected structures. The configuration shown in the top panel is characterized by an extended

disordered region in the bottom-right part of the nano-particle. At a variance, two smaller disordered regions characterize the second configuration shown in bottom panel, respectively in the bottom-right and top-left part of the nano-particle. Both configurations should be considered for the correct evaluation of the integral appearing in Eq. 1 corresponding to the same value of $\mathcal{Q}_6^*$. While these additional "slow" but unbiased degrees of freedom most likely affect the mechanism of nucleation of an ordered phase within the disordered nano-particle (and vice versa), our description of the temperature-induced disorder-to-order transition depends only on the relative stability of the initial and final metastable states (which are adequately described by the $\mathcal{Q}_6^*$ and $\mathcal{R}^*$ collective coordinates). The difference of free energy between the two states can be computed by integrating the mean force along whatever path connecting them. We can therefore still follow the original plan, namely computing and integrating the mean force on $\mathcal{Q}_6^*$ at fixed values of $\mathcal{R}^*$, provided that we can accurately compute the integral above.

We solved the problem of poor sampling by combining biased MD with the replica exchange method [13]. This technique consists in running several MD simulations at different temperatures in parallel and, from time to time, to swap the current microstate (i.e. the instantaneous set of atomic positions and momenta) between two parallel runs. The swapping is accepted/rejected according to a Metropolis Montecarlo criterion, namely with the probability $p = \min\{1, \exp[(E_{T_i} - E_{T_j})(1/K_b T_i - 1/K_b T_j)]\}$, where E_{T_i} and E_{T_j} are the energy of the two microstates respectively at the temperature T_i and T_j, and K_b is the Boltzmann constant. If the swapping is accepted, then the microstates corresponding to temperatures T_i and T_j are simply interchanged. If the swapping is rejected, the microstates are further aged at their own temperature. The key feature of this method is that the sampling of the system phase space obtained by the piece-like replica exchange trajectories is consistent with the canonical probability density function at each the target temperatures. However, since the individual pieces of the replica exchange trajectories are obtained by swapping from higher temperatures, they more likely overcome possible free energy barriers. In short: the replica exchange trajectories are ergodic.

D. Simulation protocol

The simulations proceed as follows. We run in parallel eight biased MD simulations at different temperatures (ranging from 500 K and 2000 K) but at the same target value of $\mathcal{Q}_6^*$ and $\mathcal{R}^*$. After a relaxation time, in which the swapped trajectories reach the thermal equilibrium at the new temperature, we use these trajectories to compute the integral of Eq. 1. In principle, the replica exchange method implies the extra cost of running several MD simulations at different temperatures. However, since we are interested in computing the free energy at all these temperatures we rather took advantage by following this procedure. In practice, we implemented the replica exchange/biased MD scheme in our CMPTool code [14, 15] by adopting a two-fold parallel scheme. Since the replica exchange protocol involves a minimal level of synchronization and interaction among the independent biased MD runs, parallelism is here implemented at a level of scripting language. However, as mentioned above, each individual MD simulation is computationally intensive as the samples contains up to ≈ 12000 atoms. Therefore, each MD simulation is a parallel run implemented by the Message Passing Interface (MPI) API [16]. Each MPI simulation was ran on eight cores and, therefore, the complete replica exchange/biased MD simulation was globally executed on 64 cores. One advantage of this approach is that it works well also on non-tightly connected cluster of multicore/multisocket machines. For example, part of our simulations were ran on a cluster of quad-core/dual-socket compute nodes interconnected via gigabit Ethernet.

IV. RESULTS.

A. Order-disorder phase change.

Before presenting our results, let us summarize the experimental findings we aim to interpret atomistically. By comparing Energy Filtered Transmission Electron Microscopy (EFTEM) and Dark-Field Transmission Electron Microscopy (DFTEM) images in Si-rich SiO_x samples it was shown that Si nano-particles start to form at 1000°C [7]. At this temperature they all are amorphous, while at 1100°C about one third become crystalline. By further increasing the annealing temperature by 50°C, the fraction of crystalline nano-particles rises up to 60%, while the average size of the nano-particles and the distribution of their size remains almost unchanged. Finally, at the annealing temperature of 1250°C 100%

of nano-particles are crystalline. At this temperature the average size is slightly increased, but the particle size distribution is still largely superimposed to the distributions observed at 1100°C and 1150°C. It was also found that the system has reached the thermodynamic equilibrium with respect to the amorphous vs. crystalline population. Similar investigations have been performed on Si/SiO_2 multilayers[7] where the growth of the crystalline fraction with the annealing temperature is even more sudden: the degree of crystallinity increases from about 15% to 90% when the annealing temperature is increased from 1100°C to 1200°C. Also in this case it was demonstrated that the samples are at the equilibrium.

We now turn to the results of our simulations. In Fig. 2 are shown the free energy curves of Si nano-particles of size $\mathcal{R}^* = 0.8$ nm, $\mathcal{R}^* = 1.3$ nm, and $\mathcal{R}^* = 1.8$ nm at various temperatures in the range 227°C - 1477°C (please note that calculation were performed in Kelvin while the results are presented in Celsius for homogeneity with available experimental data). It is worth mentioning that we computed this curves both starting from the crystalline region (high $\mathcal{Q}_6$) and going toward the amorphous region (low $\mathcal{Q}_6$) and vice versa without observing any significant difference. In other words, we did not observe any hysteresis affecting our results. Our simulations provide a qualitative but sharp picture, namely: for small nano-particles ($\mathcal{R}^* = 0.8 - 1.3$ nm) at low temperature (T < 727°C) the most stable configuration corresponds to a disordered phase, while the crystalline state is found to be more stable at higher temperatures. On the contrary, for larger particles ($\mathcal{R}^* \geq 1.8$ nm) this behavior is inverted resulting similar to bulk-like conditions: at low temperatures (T < 977° C) the crystalline phase is the most stable one, while the disordered phase is preferred at higher temperatures. Interestingly enough, for small nano-particles the equilibrium temperature (i.e. the temperature at which the free energy of the disordered and ordered phase are the same) decreases with the increase of the size of the nano-particle. This is indeed an effect of the steady increase of stability of the crystalline phase with respect the disordered one with the size of the nano-particles.

Our simulations further provide the following all-atom picture, consistent with the experimental results. At low annealing temperature the nano-particles are small and amorphous as, due to the inversion of stability with respect to bulk-like systems, this is thermodynamically the most stable phase. At moderately higher temperatures the size and the size distribution of the nano-particles is unchanged and the largest particles in the sample transform from amorphous to crystalline, the most stable phase at this temperature. By further

increasing the temperature the average size of the nano-particles increases and the larger nano-particles tend toward the crystalline state (i.e. they follow the change in stability from disorder to order, as induced by their growing size). On the other hand, the smaller particles undergo a disorder-to-order transition due to the increase of the temperature and the inversion of the stability with respect to the bulk-like system. Even in this case they eventually crystallize.

B. Structural trends.

Fig.2 contains also information on the structural differences among nano-particles with unsimilar size. These information are provided by the values of $\mathcal{Q}_6^*$ corresponding to the local minima of the free energy. Let us indicate such values as $\mathcal{Q}_6^d(\mathcal{R}^*, T)$ and $\mathcal{Q}_6^c(\mathcal{R}^*, T)$, respectively for the disordered and crystalline phase respectively. We remark that the $\mathcal{Q}_6^d(\mathcal{R}^*, T)$ turns out to be essentially independent from both the size and the temperature. This indicates that there is essentially no effect on the ordering by these parameters in the disordered phase. This is because in disordered (amorphous) Si there is only short range order which is hardly affected by the size of the nano-particle and by the temperature. On the contrary, $\mathcal{Q}_6^c(\mathcal{R}^*, T)$ is affected by both the temperature and the size. In the following we shall compare the $\mathcal{Q}_6^c(\mathcal{R}^*, T)$ corresponding to temperatures well within the domain of stability of the crystalline phase, namely 1227 °C, 977 °C and 477 °C corresponding to the 0.8 nm, 1.3 nm and 1.8 nm nano-particles, respectively. The values of $\mathcal{Q}_6^c(\mathcal{R}^*, T)$ are 0.18, 0.27 and 0.33 for the 0.8 nm, 1.3 nm and 1.8 nm nano-particles, respectively, clearly indicating that the order increases for larger dots tending to the bulk value ($\mathcal{Q}_6 \approx 0.63$ at $T = 0$ K and $\mathcal{Q}_6 \approx 0.57$ at $T = 1000$ K). The $\mathcal{Q}_6$ difference between bulk Si and crystalline nano-particles possibly stems from two effects. On the one hand, this difference might be due to the presence of the interface: atoms at the interface have a different environment from atoms in the core and this reduces the total $\mathcal{Q}_6$. On the other hand, the difference could be due to a distortion of the core of the nano-particle or to the presence of a significant number of localized as well as extended defects in the internal region.

Experimental results on Si nano-particles and, more in general, on confined systems, indicate that indeed the degree of order decreases in going from the centre to the surface of the cluster [17, 18]. In order to clarify this issue we computed the $\mathcal{Q}_6$ by including only

atoms falling within a given distance R from the centre of the nano-particle ($\mathcal{Q}_6^c(R;\mathcal{R}^*)$). The top panel of Fig. 3 demonstrates that the degree of order as measured by the $\mathcal{Q}_6^c(R;\mathcal{R}^*)$ decreases in going from the center to the periphery of the nano-particles. Once again, this result is consistent with the experimental picture of Ref. [17, 18].

Present results suggest that well established theories for modeling the nucleation of new phases, such as the classical theory of nucleation (see [19]), are inadequate in the case of formation of Si nano-particles in amorphous silica. In fact, several results contrast with the basic assumption of these theories. Perhaps the most relevant one is that Si nano-particles are initially formed amorphous and then transformed into crystalline, as shown by experiments and by now understood by our simulations. As a consequence, the chemical potential is not constant during the nucleation and growth of the nano-particle, as assumed in the classical nucleation theory. In addition, the results shown in Fig. 3 also suggest that: i) when the nano-particle is in the crystalline phase the structure as described by the $\mathcal{Q}_6^c$ parameter is different from the bulk one and therefore the chemical potential should differ from the bulk value as well; ii) the $\mathcal{Q}_6^c$ changes in going from the center to the periphery of the nano-particle and therefore the chemical potential will not be constant within the nano-particle; and iii) $\mathcal{Q}_6^c$ depends on the size of the nano-particle and therefore the chemical potential and the surface free energy change during the nucleation process.

Another interesting conclusion can be achieved by reporting the $\mathcal{Q}_6^c(R;\mathcal{R}^*)$ versus $\mathcal{R}^* - R$ (i.e. the distance from the interface), as shown in the bottom panel of Fig. 3. From this plot we conclude that far enough from the interface the degree of order is independent of the nano-particle size. On the other hand, $d\mathcal{Q}_6^c(R;\mathcal{R}^*)/dR$ strongly depends on the size of the nano-particle close to the interface. A possible qualitative interpretation relies on the assumption that the matrix is a source of stress on the nano-particle. Such a stress field generates a distortion (with respect to the bulk configuration) which is randomly distributed on the interface atoms. This prevents the reconstruction that normally occurs at surfaces. Furthermore, since the number of interface atoms among which the stress is distributed changes as a function of the size of the nano-particle (in particular is proportional to $(\mathcal{R}^*)^2$), the degree of distortion at the interface is a function of the nano-particle size. The stress induced by the matrix is balanced by the opposite action of the crystalline core of the nano-particle. Let us call this effect "inertia" of the nano-particle against the distortion. This phenomenon is as well function of the area of the layer which is subject of this inertia

which, for a given distance from an interface, is stronger for smaller nano-particles. The overall effect of the two contrasting phenomena is inducing a disorder distributed over few layers beyond which the original disorder is recovered. For the reasons described above, these features are higher for smaller nano-particles. Of course there can be cases in which the level of order in the nano-particle cannot recover the bulk value. For example, in our simulations only the largest particle recover the finite temperature bulk value in the core region.

The structural differences among the crystalline phase of the three nano-particles is also illustrated by the g(r) calculated on the biased MD trajectories (see Fig. 4). Indeed, the main difference between bulk crystalline Si and the largest nano-particle is mainly the intensity of the peaks, which however remain all well separated. In particular, the intensity of the first peak is significantly decreased but its integral is preserved. This means that the number of nearest neighbors is preserved. Indeed, the change of intensity is due to a broader distribution of the Si-Si bond length rather than an increase of the Debye-Waller factor, which is essentially unchanged between the bulk and nano-sized Si. With the shrinking of the nano-particle the second set of peaks becomes broader and less intense. However, also in the case of the 0.8 nm nano-particle, the two peaks of the second set are still visible. As for the first peak, its intensity is not significantly affected by the size of the nano-particle. These results indicate that also in small nano-particle there is still a short and medium range order. We conclude that the ordered states of the three nano-particle are crystalline states.

V. CONCLUSIONS.

Nano-sized systems are attracting much interest as in many cases their properties are different, and improved, with respect to the bulk counterpart. However, in preparing such systems it must be taken into account that also the phase diagram might strongly differ from the bulk case. In this paper we have shown that this is the case for Si nano-particles embedded in amorphous silica. In fact, at a variance from the Si bulk, the range of temperature in which the crystalline or the amorphous phase is the most stable depends on the size of the nano-particle. This fact is of paramount importance for developing new approaches for the preparation of systems of well defined structural properties. Another relevant aspect to be considered in developing nano-sized systems is that their structural properties, and therefore

possibly also other properties (like photoluminescence, etc.), are not homogeneous within the particle. However, the origin of this inhomogeneity is not the presence of localized defect, rather the structure of the system changes continuously in going from the center to the periphery of the nano-particle. This is the result of the stress field induced by the presence of the amorphous embedding matrix. This suggest that on the one hand one have to take into account this inhomogeneity when designing a new system with tailored properties; on the other hand, it could be possible to introduce dopants to increase the "inertia" of the interface to the distortion induced by the matrix, so as to keep the structure homogeneous all over the nano-particle.

VI. APPENDIX: DEFINITION OF THE $\mathcal{Q}_6(x)$ COLLECTIVE COORDINATE.

The $\mathcal{Q}_6(x)$ bond orientational order parameter has been originally introduced by Steinhard et al.[8] for bulk systems. In this paper we adapted the original definition to the case of confined systems. $\mathcal{Q}_6(x)$ is the properly normalized square modulus of the vector $\mathcal{Q}_{6m}(x)$, where m=-6, ..., +6:

$$\mathcal{Q}_6(x) = \left(\frac{4\pi}{2 \times 6 + 1} \sum_{m=-6}^{6} |\mathcal{Q}_{6m}(x)|^2 \right)^{\frac{1}{2}} \tag{2}$$

where $\mathcal{Q}_{6m}(x)$ is the normalized and weighted sum of atomic vectors $q^i_{6m}(x)$

$$\mathcal{Q}^i_{6m}(x) = \frac{\sum_{i=1}^{N} N_i q^i_{6m}(x)}{\sum_{i=1}^{N} N_i} \tag{3}$$

where N is the number of atoms and N_i is the number of nearest neighbor of the atom i. Finally, $q^i_{6m}(x)$ is defined according to the following expression:

$$q^i_{6m}(x) = \frac{\sum_{j=1}^{N_i} y_{6m}(\hat{x}_{ij})}{N_i} \tag{4}$$

where $y_{6m}(\hat{x}_{ij})$ is the spherical harmonics of degree 6 and component m computed on the solid angle formed by the distance vector $\vec{x}_{ij}$ and the reference system. The sum runs over the N_i nearest neighbor of the atom i. The sum over the component m in Eq. 2 makes the collective coordinate $\mathcal{Q}_6(x)$ rotationally invariant, i.e. independent on the orientation of the reference system.

When the system is crystalline and the temperature is 0 K the environment of all the atoms is the same and therefore $\mathcal{Q}_{6m}(x)$ are maxima as there is not interference among $q^i_{6m}(x)$. On the contrary, in a perfectly disordered system the orientation of bonds is random and therefore there is complete interference among $q^i_{6m}(x)$, and $\mathcal{Q}_{6m}(x)$ and $\mathcal{Q}_6(x)$ are zero.

In the case of confined systems we modify the original definition of $\mathcal{Q}_{6m}(x)$ by limiting the sum to just the atoms belonging to the nano-particle:

$$\mathcal{Q}_6 m(x) = \sum_{i=1}^{N} q^i_{6m}(x) \left(1 - H(|x_i^{Si} - x_c| - \mathcal{R}^*)\right) \tag{5}$$

where $H(x)$ is the Heaviside step function, that is the function such that $H(x) = 0$ if $x \leq 0$ and $H(x) = 1$ if $x > 0$, and $\mathcal{R}^*$ is the size of the given nano-particle (see Sec. Theory in the main text).

The biasing potential related to $\mathcal{Q}_6(x)$ gives rise to additional contributions to the inter-atomic forces that include the term $\nabla \mathcal{Q}_6(x)$. We have therefore the problem of computing the derivative of an Heaviside step function, which would produce an impulsive force. We solved this problem by replacing the Heaviside step function $H(x)$ with a sigmoid function $S(x)$, which makes the force no longer impulsive. For similar reasons, each term in the calculation of $q^i_{6m}(x)$ is also multiplied by a sigmoid function so as to eliminate impulsive forces when atoms enter and exit from the list of nearest neighbors of a given atom belonging to the nano-particle. In both cases, we defined the sigmoid function in term of the Fermi function

$$S(x) = 1 - \frac{1}{1 + \exp[\lambda x]} \tag{6}$$

In the expression above λ is a parameter controlling the smoothness of the sigmoid. In our case λ is chosen such that the sigmoid goes from 0.95 to 0.05 in one atomic layer (≈ 2 Å). In this way we are essentially biasing only atoms which belong to the nano-particle according to the definition $|x_i^{Si} - x_c| \leq \mathcal{R}^*$ given in the main text.

VII. APPENDIX: SMOOTH ANALYTICAL APPROXIMATION TO $\mathcal{R}(x)$.

The smooth analytical approximation to the $\mathcal{R}(x)$ is obtained in two steps: i) first we obtain an analytic (explicit) expression of $\min\{|x_c - x_i^O|\}$ as a function of the positions x_i^O,

ii) then we introduce a smooth approximation to this expression. The first step consists in recognizing the following identity:

$$\min_i\{|x_c - x_i^O|\} \equiv \sum_i |x_c - x_i^O| \prod_{j\neq i}^{N_i} H(|x_c - x_i^O| - |x_c - x_j^O|) \tag{7}$$

where $H(x)$ is the Heaviside step function. If k is the O atom closest to the center of the nano-particle, then $\prod_{j\neq i}^{N_i} H(|x_c - x_i^O| - |x_c - x_j^O|) = \delta_{ik}$, where δ_{ik} is the Kronecker symbol. Eq. 7 is the analytical expression of the collective coordinate $\mathcal{R}(x)$. A smooth approximation to $\mathcal{R}(x)$ can be obtained by replacing the Heaviside step function by a sigmoid function. In our case, the sigmoid function was expressed in term of the Fermi function:

$$S(x) = 1 - \frac{1}{1 + \exp[\lambda x]} \tag{8}$$

where λ is the parameter controlling the smoothness of the Fermi function. In our simulations λ has been chosen such that the sigmoid function goes from 0.95 to 0.05 in one atomic layer ($\approx$ 2 Å). A consequence of this replacement is that the size of the nano-particle is now defined as a weighted average of the distance of one atomic layer of oxygen atoms from the centre of the nano-particle.

---

[1] L. Pavesi, L. Dal Negro, C. Mazzoleni, G. Franzó and F. Priolo (2000) Optical gain in silicon nanocrystals. *Nature* 408:440-444

[2] F. Iacona, C. Bongiorno, C. Spinella, S. Boninelli and F. Priolo (2004) Formation and evolution of luminescent Si nanoclusters produced by thermal annealing of SiOx films. *J. App. Phys.* 95:3723-3732

[3] Stenger et al. (2008) Evolution of the optical properties of Si nanoparticles embedded in SiO2 as function of annealing conditions. *J. App. Phys.* 103:114303–1-8

[4] Y. Wakayama, T. Inokuma, S. Hasegawa (1998) Nanoscale structural investigation of Si crystallites grown from silicon suboxide films by thermal annealing. *J. Cryst Growth.* 183:124-130

[5] Inokuma et al. (1998) Optical properties of Si clusters and Si nanocrystallites in high-temperature annealed SiOx films. *J. App. Phys.* 83:2228-2234

[6] Y.Q. Wang, R. Smirani and G.G. Ross (2006) The formation mechanism of Si nanocrystals in SiO_2. *J. Cryst. Growth* 294:486-489

[7] Boninelli et al. (2007) Formation, evolution and photoluminescence properties of Si nanoclusters. *J. Phys.: Cond. Mat.* 19:225003–1-24

[8] P. J. Steinhardt, D. R. Nelson and M. Ronchetti (1983) Bond-orientational order in liquids and glasses. *Phys. Rev. B* 28:784-805

[9] S. R. Billeter, A. Curioni, D. Fischer, W. Andreoni (2006) Ab initio derived augmented Tersoff potential for silicon oxynitride compounds and their interfaces with silicon. *Phys. Rev. B* 73:155329–1-15

[10] S. R. Billeter, A. Curioni, D. Fischer, W. Andreoni (2009) Erratum: Ab initio derived augmented Tersoff potential for silicon oxynitride compounds and their interfaces with silicon [Phys. Rev. B 73, 155329 (2006)]. *Phys. Rev. B* 79:169904-1

[11] M. Ippolito, S. Meloni, L. Colombo (2008) Interface structure and defects of silicon nanocrystals embedded into a-SiO_2 *Appl. Phys. Lett.* 93:153109

[12] L. Maragliano and E. Vanden-Eijnden (2006) A temperature accelerated method for sampling free energy and determining reaction pathways in rare events simulations. *Chem. Phys. Lett.* 426:168-175

[13] D. J. Earlab and M. W. Deem (2005) Parallel tempering: Theory, applications, and new perspectives. *Phys. Chem. Chem. Phys.* 7:3910-3916

[14] Meloni et al. (2005) Computational Materials Science application programming interface (CMSapi): a tool for developing applications for atomistic simulations. *Comp. Phys. Comm.* 169:462-466

[15] https://cmsportal.caspur.it/index.php/CMPTool

[16] http://www.mcs.anl.gov/research/projects/mpi/

[17] Daldosso et al. (2003) Role of the interface region on the optoelectronic properties of silicon nanocrystals embedded in SiO_2. *Phys. Rev. B* 68:085327–1-8

[18] U. Gasser, E. R. Weeks, A. Schofield, P. N. Pusey, D. A. Weitz (2003) Real-Space Imaging of Nucleation and Growth in Colloidal Crystallization. *Science* 292:258-262

[19] Kelton KF and Greer AL (2010) in *Nucleation in Condensed Matter*, eds Kelton KF, Greer AL (Elsevier, Amsterdam), pp 19-52.

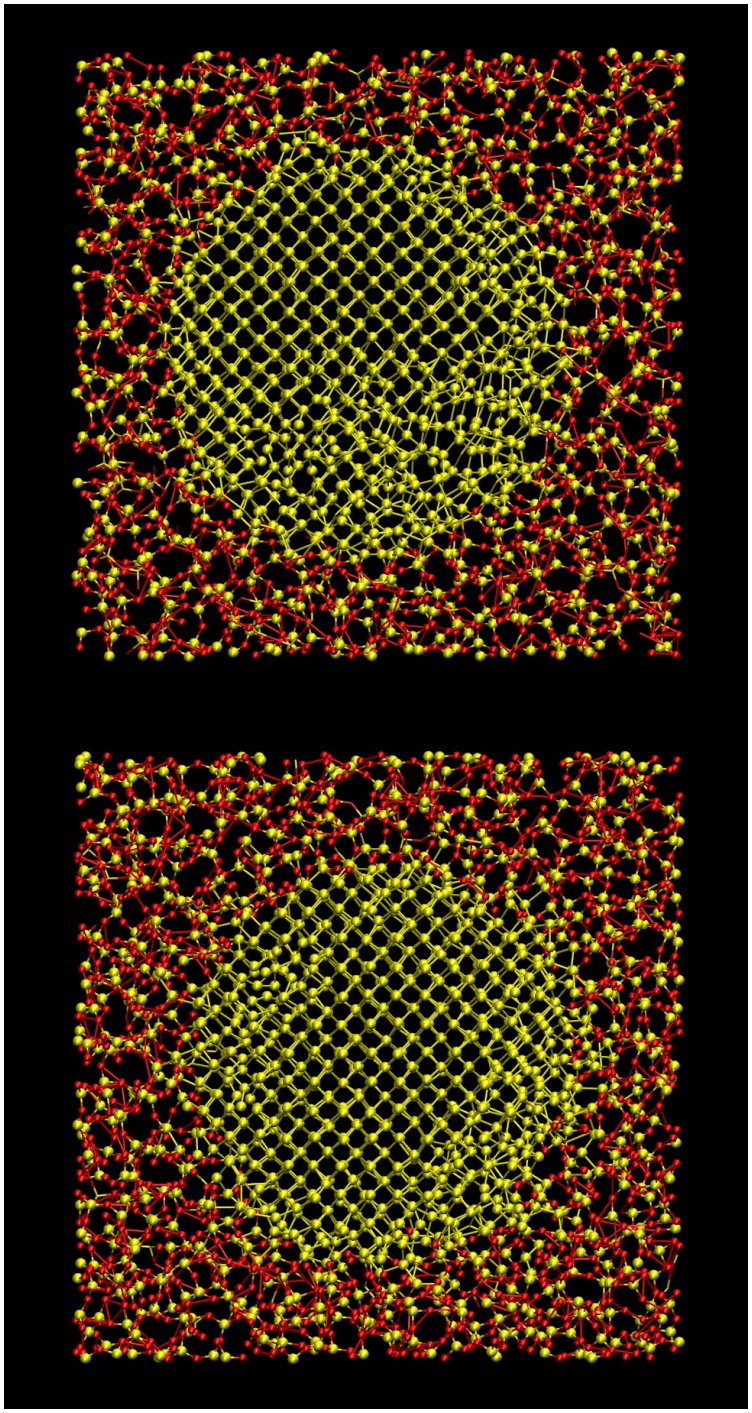

FIG. 1: Two different configurations of an embedded silicon nano-particle with radius as large as 0.18 nm. They both correspond to $\mathcal{Q}_6^* = 0.19$. Oxygen atoms are displayed in red and Silicon atoms in yellow. In order to improve the readability, only the atoms laying within a 15 Å-thick slice are drawn.

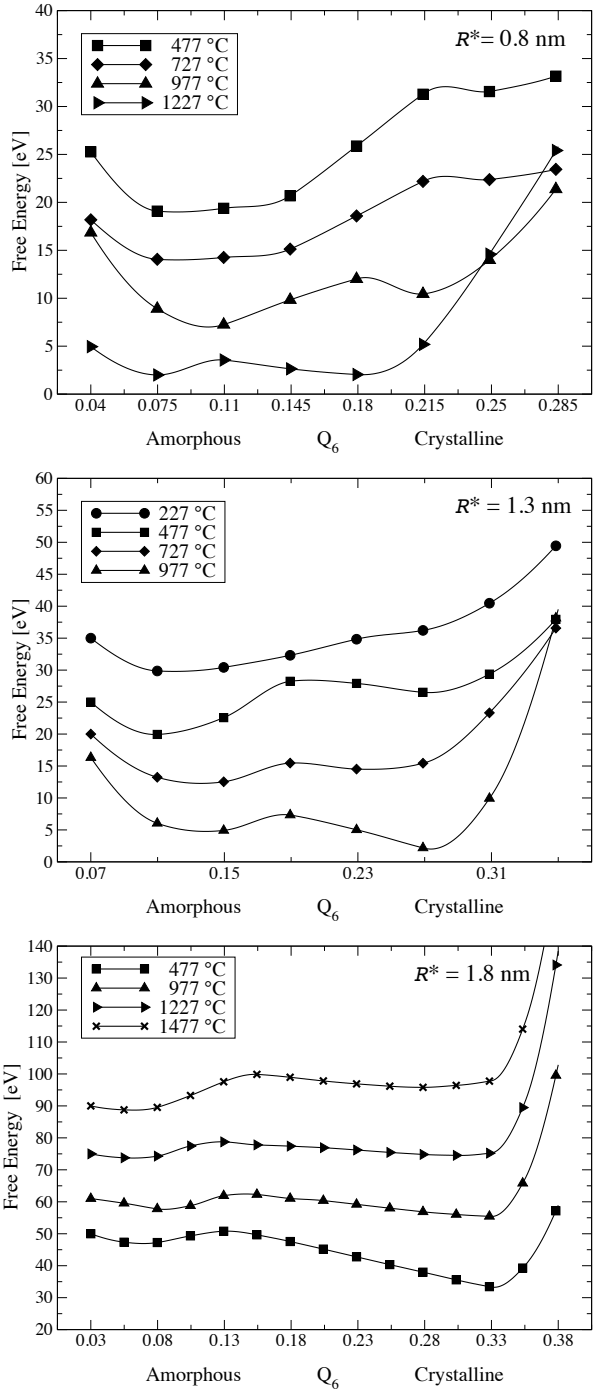

FIG. 2: Free energy vs $\mathcal{Q}_6$ curves for nano-particles with radius 0.8 nm (top), 1.3 nm (middle) and 1.8 nm (bottom). The curves are shifted to improve readability.

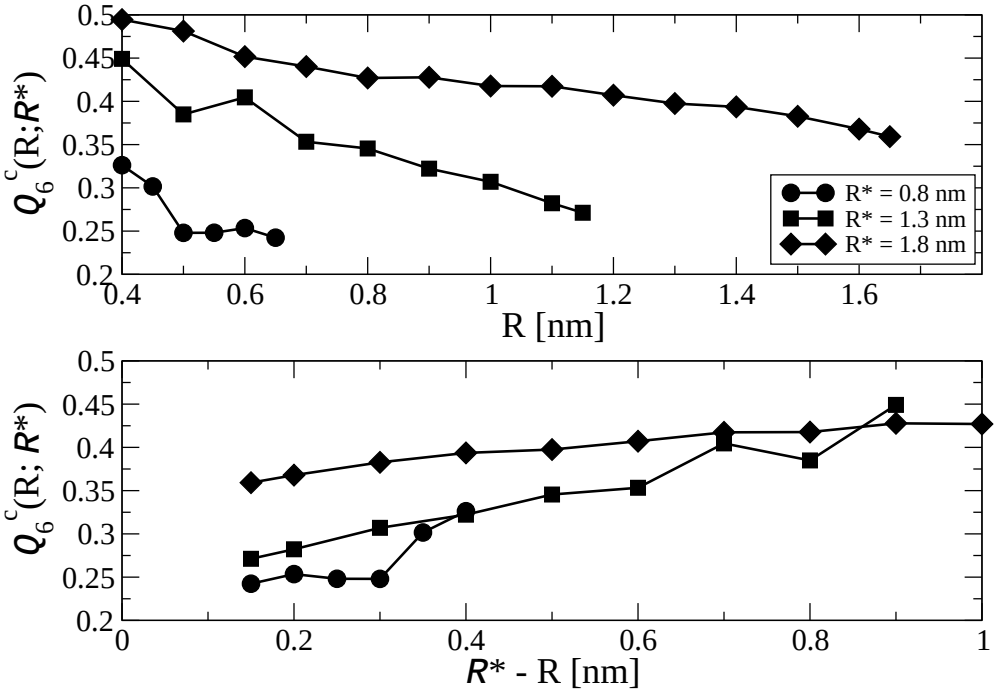

FIG. 3: (top) $\mathcal{Q}_6^c$ as a function of the distance R from the center of the nano-particles. (bottom) $\mathcal{Q}_6^c$ as a function of the distance from the interface.

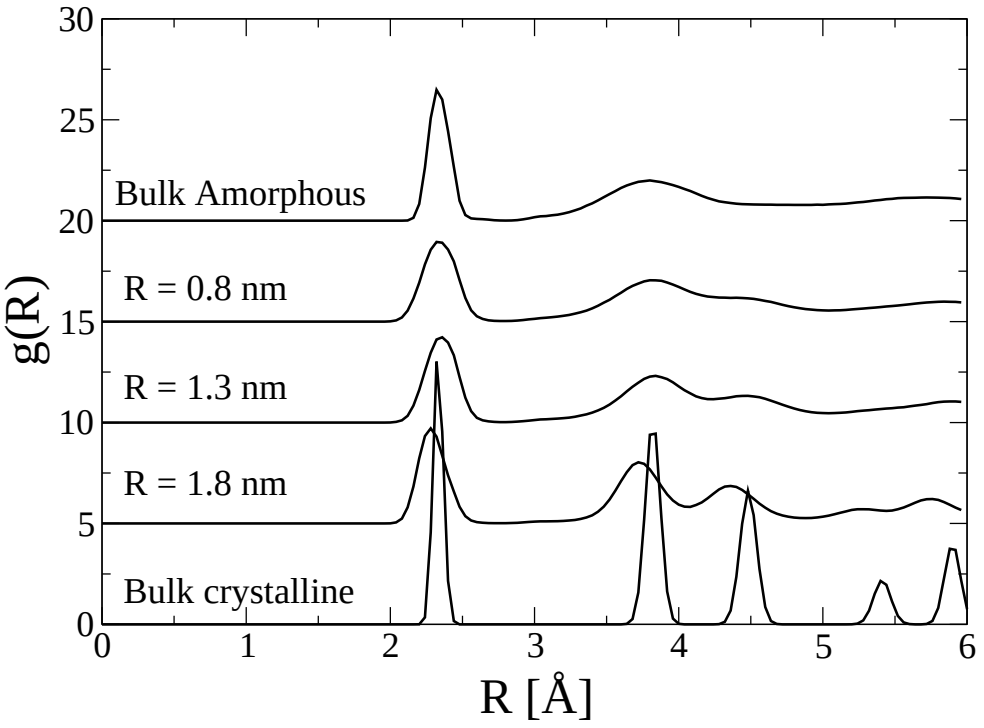

FIG. 4: Pair distribution function of nano-particles of different size. For comparison, the g(r) of bulk silicon is also reported.